Int. J. Electrochem. Sci., 16 **(2021)** Article ID: 21034, doi: 10.20964/2021.03.25

International Journal of
ELECTROCHEMICAL
SCIENCE
www.electrochemsci.org

Effect of Turbulent Flow on Corrosion Behavior of 6.5Cr Steel in CO_2-Containing Environment

Bei Wang[1*], *Yun Wang*[1], *Qingping Li*[2], *Lihua Hu*[2], *Wei Chang*[2], *Huixin Li*[2], *Minxu Lu*[1]

[1] University of Science and Technology Beijing, Beijing 100083, China
[2] CNOOC Research Institute, Beijing, 100028, China
[*]E-mail: 247776086@qq.com

Received: 29 April 2020 / *Accepted:* 29 December 2020 / *Published:* 31 January 2021

The effect of turbulent flow on the corrosion behavior of 6.5Cr steel in CO_2-saturated oil field formation water was examined using a rotating cylinder electrode. Electrochemical measurements demonstrated that increasing the flow rate could decrease the corrosion rate of 6.5Cr steel. When the rotation rate of the rotating cylinder electrode reached 2000 rpm, 6.5Cr steel could be passivated. Surface characterization and ion analysis results showed that increasing flow rate reduced Fe^{2+} concentration in the solution near the steel surface, inhibited $FeCO_3$ deposition, and then increased $Cr(OH)_3$ concentration in a corrosion film.

Keywords: Cr-bearing alloy steel, Rotating cylinder electrode, CO_2 corrosion, Passivity, Flow rate

1. INTRODUCTION

Internal pipeline corrosion caused by $CO_2$is one of the primary concerns during the production and transportation of oil and gas [1]. Carbon steel is the most widely used pipeline material in the oil and gas industry [2-6]. However, a high turbulent flow rate can be detrimental to the corrosion film and corrosion inhibitor film and thereby increase erosion risk [7-10].

Low Cr-bearing alloy steel, which boasts an excellent performance to price ratio and improved CO_2 corrosion resistance, can replace carbon steel for use in pipelines [11-13]. Experimental and field data published in other research have indicated that the corrosion rate of low Cr-bearing alloy steels generally decreased while pitting corrosion resistance improved with increasing Cr concentration [14,15]. Numerous researchers have asserted that low Cr-bearing alloy steel has excellent corrosion resistance due to the formation of a more protective Cr-rich corrosion film [16-19]. Some studies [20,21] have shown that the corrosion film of 3Cr steel consists of $Cr(OH)_3$ and $FeCO_3$. Compared with the crystalline corrosion film of carbon steel, which of 3Cr steel is amorphous, is much denser and more protective. Relevant studies have reported the formation of a film, primarily comprised of $Cr(OH)_3$, on low Cr-bearing alloy steels (3-6.5Cr), resulting in the pseudopassivation in a CO_2 corrosion environment. The excellent corrosion resistance of low Cr-bearing alloy steel is mainly related to the pseudopassivation.

Flow rate has an important effect on the morphology and properties of a $FeCO_3$ scale on carbon steel [22-24]. However, few investigations have been conducted on the influence of flow on the corrosion behavior and corrosion product performance of low Cr-bearing alloy steel. Guo et al. [25] indicated that flow can increase the corrosion rate of 3Cr steel, but also promote the enrichment degree of Cr(OH)3 in the product film. Furthermore, flow suppressed the presence of potential pits and generated a flatter film/steel interface. Jiang et al. [26,27] reported that Cr is beneficial to improve the resistance to flow accelerated corrosion of low alloy steel caused by the inhibition of a cathodic reaction in an O_2-containing environment. The addition of Cr generates amorphous products in a rust layer.

There are few systematic studies on the corrosion behavior of Cr-bearing alloy steel, whose Cr content is slightly higher than that of low Cr-bearing alloy steels (1%–5%). The corrosion behavior and mechanism of low Cr-bearing alloy steels under different flow conditions in a CO_2-containing environment are still not well understood. Therefore, this study focused on understanding the effect of flow on the corrosion behavior and mechanism of 6.5Cr steel in a CO_2-containing environment. This study can promote the application of Cr-bearing alloy steels in the oil and gas industry

2. EXPERIMENT

2.1. Material and solution

The sample used in this study was 6.5Cr steel, the elemental composition (wt.%) of which is provided in Table 1. The samples were ground to 800# by silicon carbide paper and then rinsing with distilled water and alcohol. Table 2 presents the composition of the test solution. The solution was deaerated using pure CO_2 for 24 h before the test. The pH of the solution was 5.6.

Table 1. Elemental composition of 6.5Cr steel (wt.%)

Element	C	Si	Cr	Mn	Mo	Nb	V	Ti	Fe
Content	0.07	0.20	6.50	0.55	0.15	0.03	0.03	0.03	Bal

Table 2. Composition of the test solution

Composition	NaCl	KCl	$NaHCO_3$	$CaCl_2$	$MgCl_2·6H_2O$	Na_2SO_4
Content ($mg·L^{-1}$)	25318.99	643.75	519.15	2747.25	1920.03	196.73

2.2. Electrochemical measurements

The rotating cylinder electrode (RCE) is an ideal device for simulating the turbulent flow. By increasing the rotation rate, a higher turbulent velocity can be easily obtained. The electrochemical measurements were performed within a glass cell with a conventional three-electrode system by using a Gamry Interface 1000 electrochemical workstation. The volume of the test solution was 800 mL. The working electrode was a 6.5Cr rotating cylinder, with a diameter, length, and electrode surface area of 12 mm, 8 mm, and 3 cm^2, respectively. A platinum sheet was used as a counter electrode and a saturated calomel electrode (SCE) was used as a reference electrode. Potentiodynamic polarization curves were obtained after 1 h or 24 h of immersion in a solution with different rotation rates (0, 1000, and 2000 rpm) at a voltage ranging from −350 to 350 mV [vs. open circuit potential (OCP)] by using a scan rate of 0.5 mV/s. To study the corrosion processes of 6.5Cr steel under different rotation rates, electrochemical impedance spectroscopy (EIS) measurements were performed using alternate current signals, with a peak-to-peak amplitude of 10 mV at an OCP in a frequency range of 100 kHz to 5 mHz. To study the passivation process of 6.5Cr steel at rotation rates of 2000 rpm, EIS tests were conducted at OCP potentials of −620, −550, and −525 mV (vs. SCE) after the specimens were prefilmed through potentiostatic polarization at the corresponding potentials. The tests were performed at 80°C in a CO_2-saturated solution under atmospheric pressure.

The X-ray photoelectron spectroscopy (XPS) of the film was examined using a ThermoEscalab 250Xi instrument. The morphology of corrosion film was examined using a JSM-6510A SEM, and energy dispersive X-ray spectroscopy (EDS) were examined using a JED-2300 EDS. An inductively coupled plasma optical emission spectrometer Agilent 5110DVD ICP-OES was used to measure the Fe^{2+} concentration in the solution after the test.

3. RESULTS AND DISCUSSION

3.1. Open circuit potential

Fig. 1 displays the OCPs of 6.5Cr steel at different rotation rates as a function of time. For 0 and 1000 rpm, the OCPs of 6.5Cr steel sharply decreased from the value of −0.710 V at the initial stage and were then asymptotically stabilized at −0.726 and −0.713 V, respectively. The OCP of 6.5Cr steel at 2000 rpm abruptly increased from −0.722 to −0.686 V at the initial stage and was then gradually stabilized at −0.680 V, which was a considerably higher OCP than those measured at 0 and 1000 rpm. Zhu and Xu found that with the development of corrosion, the OCP of low-Cr alloy steel will become positive, leading to pseudopassivation, thus increasing the corrosion resistance of low-Cr alloy steel [14,28].

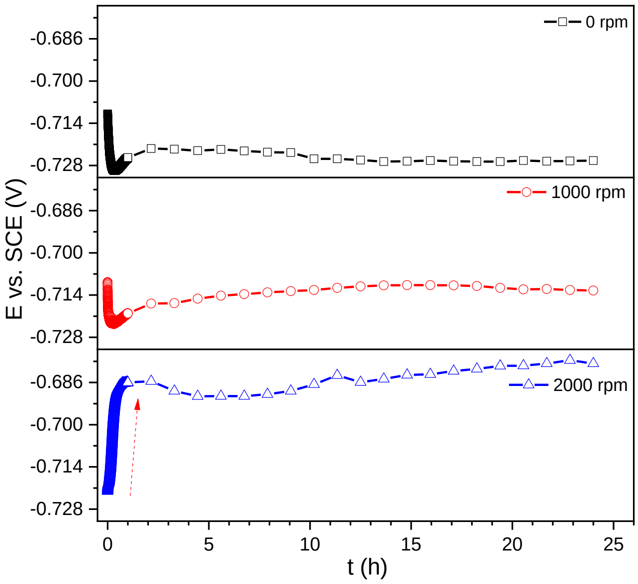

Figure 1. OCP monitoring curves of 6.5Cr steel measured at 0, 1000, and 2000 rpm

3.2. Electrochemical impedance spectroscopy

The corrosion process of 6.5Cr steel under different rotation rates was periodically investigated through EIS. Fig. 2a shows the Nyquist plots obtained at 0 rpm after 1, 3, 5, 9, 12, 18, and 24 h of immersion, with the characteristics of two typical capacitance loops. The impedance gradually increased in an initial stage and was stabilized after 3 h, and thus the behavior was due to the growth of a corrosion film on the substrate. Fig. 3 presents the equivalent circuits for EIS fitting. R_s, R_{pore}, and CPE_{film} denote the solution resistance, pore resistance of the corrosion film, and constant phase element of the corrosion film capacitance, respectively. Electrochemical processes at the interface are represented by R_{ct} and CPE_{dl}, which denote the charge transfer resistance and electric double-layer capacitance, respectively. Y_o and n are the parameters of the constant phase element. For 1000 rpm, Fig. 2b shows that the shape of the Nyquist plot obtained in the initial stage (1–5 h) was consistent with that of 0 rpm and was fitted with the equivalent circuit model as shown in Fig. 3a. An inductive loop was observed, and the Nyquist plot revealed three-time constants after 9 h. This behavior was attributed to the dissolution of the corrosion film and the adsorption of the intermediate products [1]. The EIS plots were fitted with the equivalent circuit model as shown in Fig. 3b. R_L and L were the inductive resistance and inductance, respectively. For 2000 rpm, Fig. 2c indicates that the shape of the Nyquist plot measured in the initial stage (1–5 h) was consistent with that at 0 and 1000 rpm and was fitted with the equivalent circuit model as shown in Fig. 3a. With time, the low-frequency capacitance loop was converted into a short straight line with a 45° angle against the real axis, which indicated a diffusive process of H^+ and HCO_3^-. The EIS plots were fitted with the equivalent circuit model as shown in Fig. 3c. W denotes Warburg impedance. Table 3 lists the fit values of the impedance spectra.

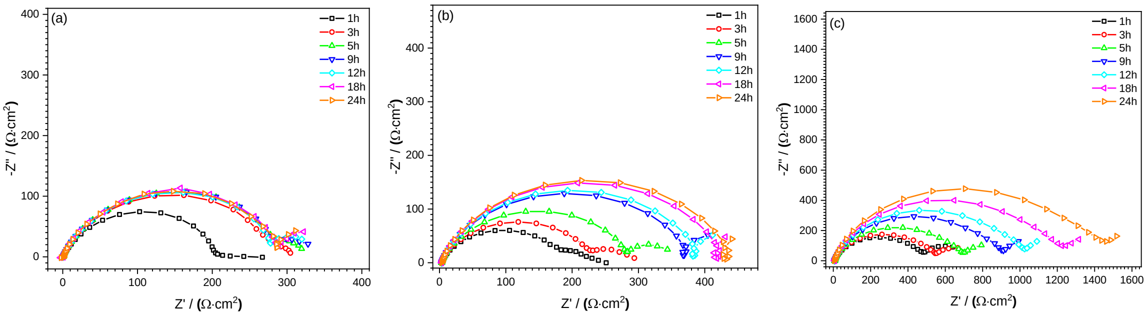

Figure 2. Nyquist plots of 6.5Cr steel obtained at (a) 0 rpm; (b) 1000 rpm; (c) 2000 rpm

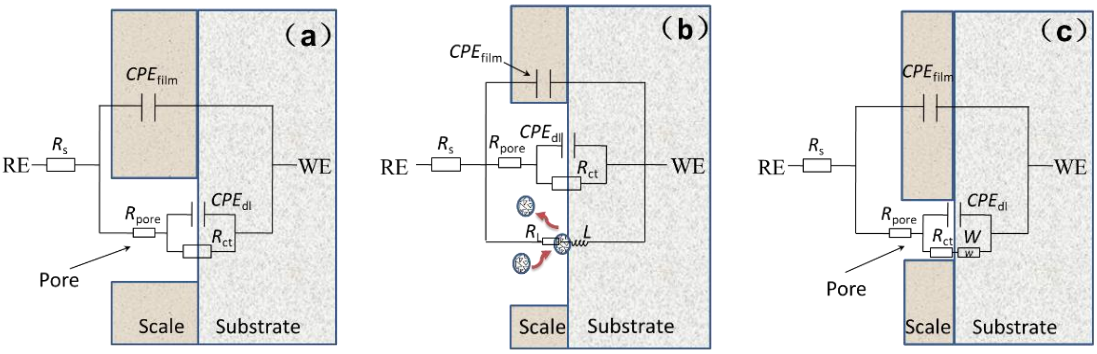

Figure 3. Equivalent circuits employed to model the EIS plots in Figure 2.

The polarization resistance (R_p), which is the sum of R_{pore} and R_{ct}, was inversely proportional to the corrosion rate [29]. For carbon steel or low Cr-bearing alloy steel, the pores in the corrosion film provide channels for the corrosion medium. Thus, the resistance of the pores in the corrosion film (R_{pore}) can be used to characterize the corrosion product film [30]. Fig. 4 presents R_{pore} and R_p obtained from Table 3. R_{pore} and R_p measured at 0 and 1000 rpm increased with time in the initial stage and were then stabilized, whereas for 2000 rpm, R_{pore} and R_p keep increasing over time. The protection performance of the corrosion film increased and the corrosion rate decreased because the corrosion film grew with time. R_p was dependent on the material, corrosion film, and corrosion condition. For 6.5Cr steel, the increasing flow rate was detrimental to R_p. However, Fig. 4c shows that R_{pore} and R_p increased with increasing rotation rate. In particular, for 2000 rpm, R_{pore} and R_p were considerably higher than that measured at 0 and 1000 rpm, and the slope of R_{pore} and R_p was considerably more positive. The increasing rotation rate was advantageous for the precipitation of the improved corrosion film.

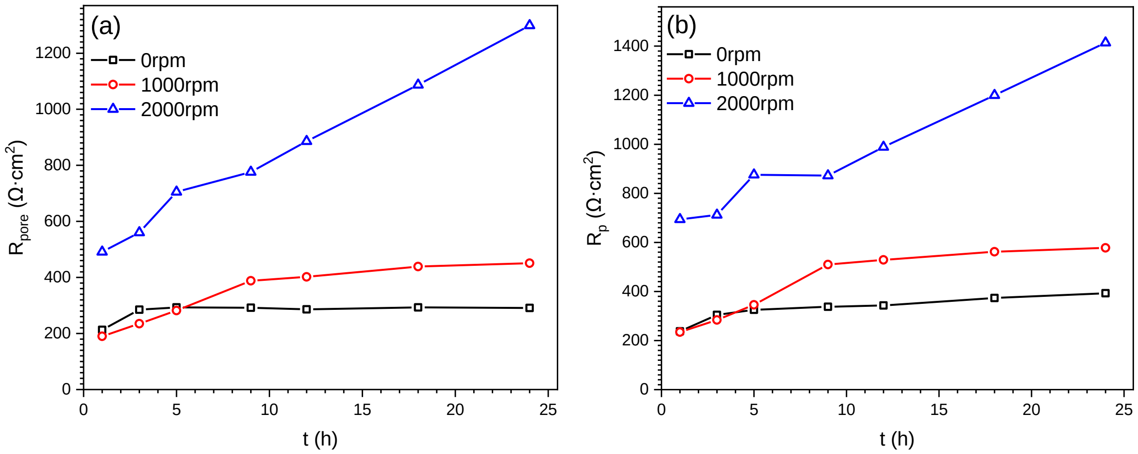

Figure 4. The R_{pore} value (a) and R_p value (b) obtained from the EIS results

Table 3. Fit values of the impedance spectra of Fig. 2.

Rotation rate	Immersion time, h	R_s,Ω·cm²	CPE$_{film}$		R_{pore},Ω·cm²	CPE$_{dl}$		R_{ct},Ω·cm²	W, ×10^{-2} Ω^{-1}·cm^{-2}s^n	R_L,Ω ·cm²	L,H
			Y_1,μΩ^{-1}·cm^{-2}s^n	n_1		Y_2,×10^{-4}Ω^{-1}·cm^{-2}s^n	n_2				
0 rpm	1	1.05	791	0.787	213	5691	1.000	24.3			
	3	0.699	687	0.788	285	4416	1.000	19.6			
	5	0.937	657	0.799	293	3757	0.975	32.5			
	9	1.07	649	0.807	292	4296	1.000	45.6			
	12	1.23	651	0.818	286	4824	1.000	56.9			
	18	1.07	684	0.821	293	6265	1.000	80.6			
	24	1.15	725	0.824	291	7731	1.000	102			
1000 rpm	1	2.60	612	0.733	190	827	0.888	44.6			
	3	2.71	552	0.744	235	1853	1.000	48.8			
	5	3.22	450	0.785	282	2609	0.989	63.8			
	9	2.58	474	0.760	388	3714	1.000	122		4498	21380
	12	2.62	460	0.762	402	4198	1.000	127		4687	24830
	18	2.28	421	0.767	439	5607	1.000	123		4964	31960
	24	2.56	408	0.769	451	5736	1.000	127		4949	36910
2000 rpm	1	5.81	372	0.738	491	870	0.919	203			
	3	4.91	382	0.728	560	1974	1.000	152			
	5	5.10	351	0.729	705	2411	1.000	171			
	9	6.99	246	0.806	776	34.6	1.000	96.3	4.23		
	12	6.82	238	0.806	886	37.5	1.000	103	4.47		
	18	6.16	231	0.800	1087	49.0	0.921	113	4.11		
	24	5.14	223	0.799	1299	68.9	0.984	115	3.69		

3.3. Potentiodynamic polarization curves

Fig. 5a and Fig.5b display the polarization curves of 6.5Cr steel measured at different rotation rates after immersion for 1 h and 24 h. Table 4 lists the electrochemical parameters obtained from the polarization curves shown in Fig. 5. The cathodic polarization curves exhibited subtle differences among various rotation rates. This behavior is attributable to H^+ and HCO_3^- being the primary ions that are reduced in the CO_2-saturated solution, and the rotation rate is less effective on the reduction reaction. For 0 and 1000 rpm, only an active-passive transition region and no passive region (i.e., pseudopassivation [14]) were observed in the anodic polarization curves of 6.5Cr steel, and the active regions overlapped. Furthermore, the current density in the active-passive transition region measured at 1000 rpm was lower than 0 rpm, and the initial potential of the active-passive transition region was more negative. For 2000 rpm, the difference was an evident passive region on an anodic polarization curve, and the current density in the active region was lower. Moreover, 6.5Cr steel was considerably easier to passivate at a high rotation rate. The previous research results of our group show that the appearance of pseudopassivation is directly related to the corrosion product film generated on its surface [31]. The results indicated that increasing the rotation rate can accelerate the transition from pseudopassivation to passivation of 6.5Cr steel. Furthermore, the potential at which passivation or pseudopassivation ended decreased with the increasing rotation rate, which indicates that the higher rotation rate can promote the destruction of the passive or pseudopassive film.

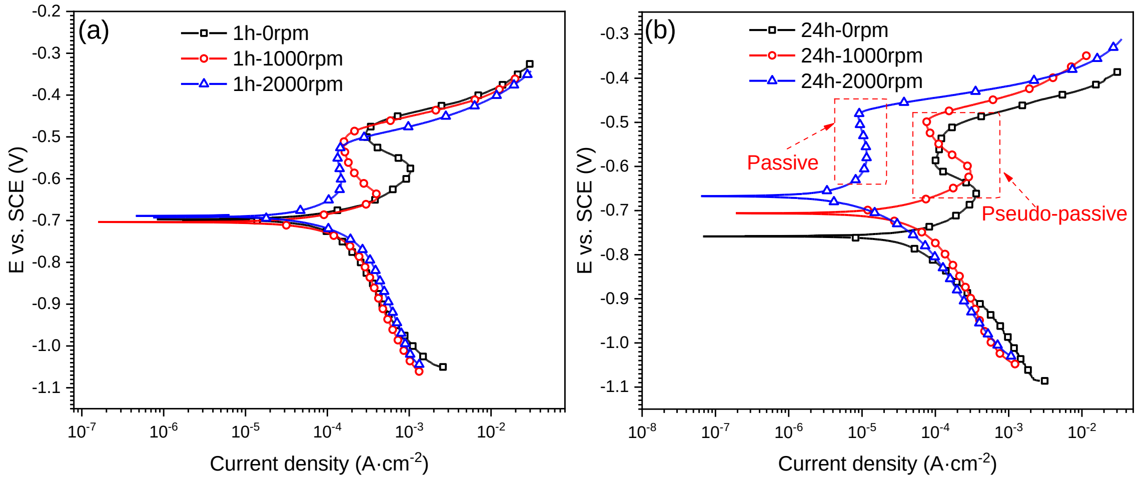

Figure 5. Polarization curves of 6.5Cr steel measured at different rotation rates after immersion for (a) 1h and (b) 24h.

Table 4. Electrochemical parameters obtained from the polarization curves shown in Fig. 5

Condition	1h-0rpm	1h-1000rpm	1h-2000rpm	24h-0rpm	24h-1000rpm	24h-2000rpm
Corrosion potential, V	-0.697	-0.704	-0.689	-0.759	-0.706	-0.667
Corrosion Current density, A/cm^2	2.99×10^{-4}	1.60×10^{-4}	1.33×10^{-4}	9.91×10^{-5}	7.61×10^{-5}	8.55×10^{-6}

Fig. 5b displays the polarization curves of 6.5Cr steel measured at different rotation rates after immersion for 24 h. Compared with the results of immersion for 1 h, the polarization curves shifted to left, and the phenomenon of passivation or pseudopassivation is more evident after immersion for 24 h. This result is consistent with that in Fig. 2. Furthermore, corrosion potential evidently increased with increasing rotation rate, which was consistent with the results of OCP monitoring. This result was closely related to the precipitation of the corrosion film [32]. The protection performance of the corrosion film improved with increasing corrosion time.

Similar to the corrosion rate of stainless steel that of 6.5Cr steel at different rotation rates can be easily calculated using the following equation:

$$V_c = \frac{A \times I_{corr}}{n \times F \times \rho} \times 87600 \qquad (1)$$

Where V_c, A, I_{corr}, n, F, and ρ are the corrosion rate of the sample in mm/y, relative atomic mass, corrosion current density in A/cm^2, number of electrons transferred; Faraday constant, and density of the sample in g/cm^3, respectively.

Fig. 6 shows that the anticorrosion performance of 6.5Cr steel improved with the increasing rotation rate. In particular, for 2000 rpm, 6.5Cr steel was passive, and the corrosion rate was considerably lower than 0–1000 rpm. The polarization result displays that 6.5Cr steel could be passive in the CO_2-containing acidic environment when the rotation rate was increased to 2000 rpm, which is considerably different from the conventional viewpoint. However, such a result is not impossible [33-35]. Wei [33] found that the corrosion rate of 6.5Cr steel hardly increased after increasing the flow rate under supercritical CO_2 conditions. Vasyliev [34] found that the flow rate increase from 0.19 to 0.45 m/s reduces corrosion rate by 2.8 times with long immersion times in hot water. To study the passivation process of 6.5Cr steel at a rotation rate of 2000 rpm, the EIS test was performed at the OCP, −620, −550, and −525 mV (vs. SCE) after the specimens were prefilmed through potentiostatic polarization at the corresponding potentials. Fig. 7 presents the results of potentiostatic polarization and EIS tests. Fig. 7 presents the equivalent circuits for EIS fitting. Table 5 lists the fit values of the impedance spectra. As shown in Fig.7b, the electrochemical impedance measured at the OCP reveals the characteristics of two typical capacitance loops; this indicates that the steel surface was covered by an intact corrosion film. When the polarization potential was increased to −620 and −550 mV, the current density sharply decreased (Fig. 7a). The second capacitance loop was gradually transformed into a straight line at an angle of 45° from the real axis, and R_{pore} and R_{ct} values increased significantly, which indicated a diffusion process caused by the formation of a passive film during anodic polarization [36].

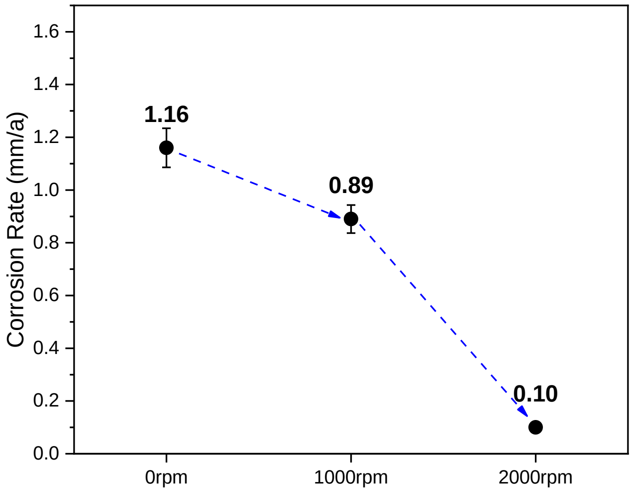

Figure 6. Corrosion rate of 6.5Cr steel measured at different rotation rates

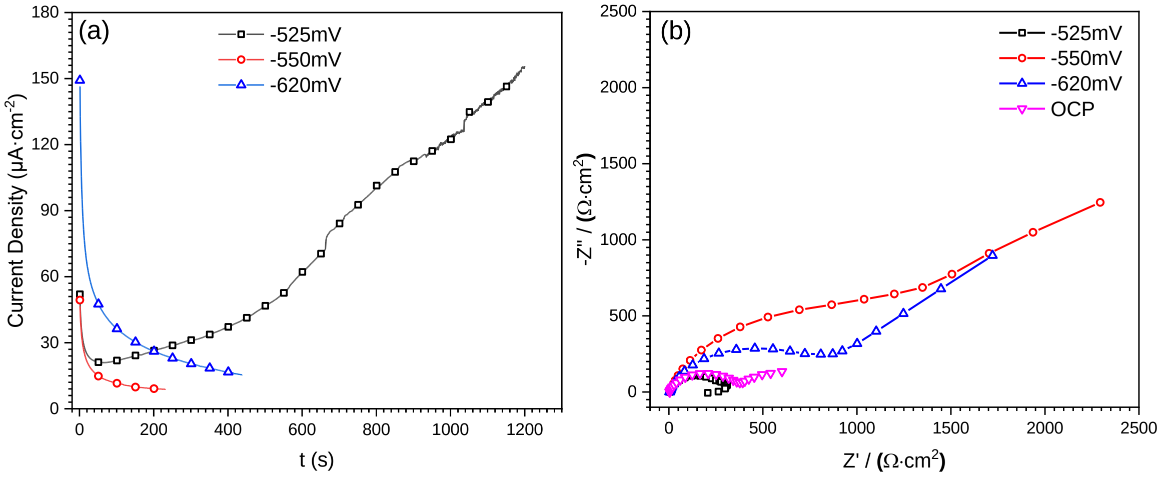

Figure 7. (a) Potentiostatic polarization curves at different potentials; (b) EIS curves measured at different potentials after potentiostatic polarization tests.

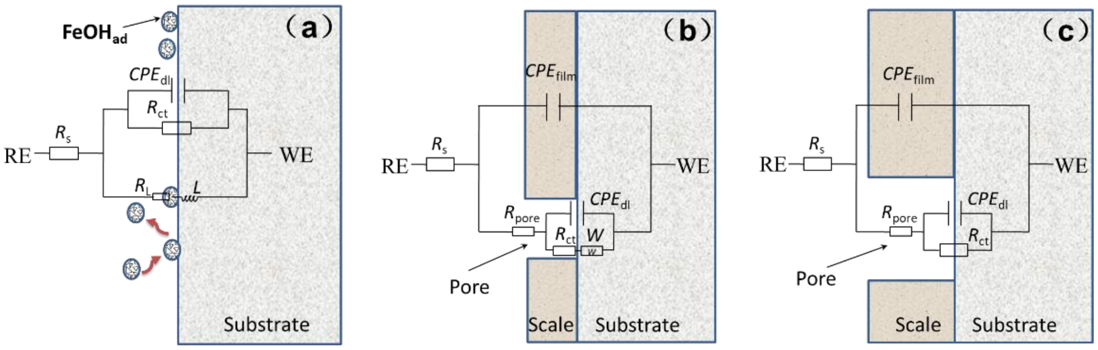

Figure 8. Equivalent circuits used for modeling the EIS results in Figure 7b.

Table 5. Fit values of the impedance spectra of Fig. 7b.

E vs.SCE, V	R_s, Ω·cm²	CPE$_{film}$		R_{pore}, Ω·cm²	CPE$_{dl}$		R_{ct}, Ω·cm²	W, ×10^{-2} Ω^{-1}·cm^{-2}s^{n}	R_L, Ω·cm²	L,H
		Y_1, μΩ^{-1}·cm^{-2}s^{n}	n_1		Y_2,×10^{-4} Ω^{-1}·cm^{-2}s^{n}	n_2				
-0.525	4.51				7.30	0.803	296		1881	39100
-0.550	3.62	469	0.780	1360	37.9	0.628	6480	1.60		
-0.620	4.50	327	0.788	805	73.0	0.646	3518	74.5		
-0.686	3.16	437	0.730	391	440	0.805	336			

When the polarization potential was increased to −525 mV, current density sharply increased, an inductive loop was observed at a low frequency, and R_p decreased significantly. These phenomena were observed because a passive film was hardly formed at a high polarization potential. This result further validated that 6.5Cr steel was passive when the rotation rate increased to 2000 rpm

3.4. Surface characterization

Some studies have proved that the corrosion resistance of low-Cr alloy steel is related to the composition and property of the Cr-rich corrosion film [14,28,31-33]. To study the passivation mechanism of 6.5Cr steel caused by the increasing rotation rate, XPS, SEM, and EDS were performed to analyze corrosion films deposited under different rotation rates.

Fig. 9 displays the XPS analysis of the corrosion film that grew on 6.5Cr steel under different rotation rates. There is no difference in the species of the corrosion products generated under three rotation rates, all of which are $Cr(OH)_3$ and $FeCO_3$. However, as shown in Fig. 9a, the peak area of $Cr(OH)_3$ increases significantly with the increase of rotation rate. It means that the flow rate does not change the species of corrosion products but the relative percentage of each product in the corrosion film.

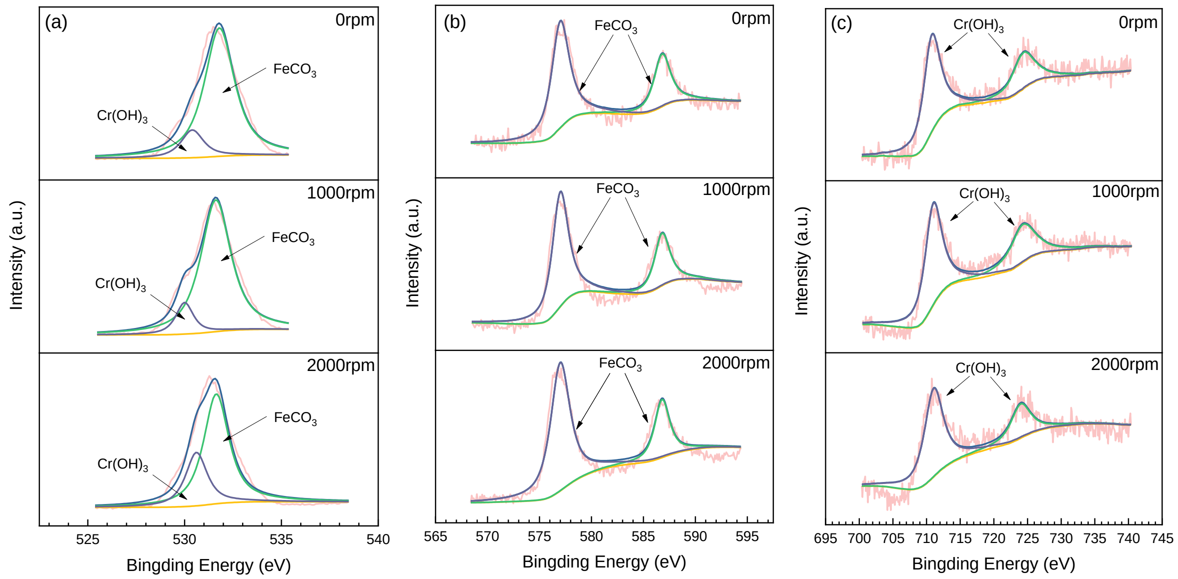

Figure 9. XPS analysis of corrosion film generated under three rotation rates （a）O 1s;（b）Fe $2p_{2/3}$;（c）Cr $2p_{2/3}$;

Fig. 10 shows the SEM and EDS analysis of corrosion film of 6.5Cr steel after immersion for 24 h under different rotation rates. Fig. 10a indicates that the corrosion film formed at 0 rpm was intact, and some cracks formed through the entire surface because of dehydration [37]. Fig.10d indicates that the corrosion film was rich in Cr. The atom% of O was 27.74%, which demonstrated that the thinness of the corrosion film was so thin that the X-ray penetrated the corrosion film and detected the signal from the matrix.

Fig. 10b displays the morphology of 6.5Cr steel after immersion for 24 h at 1000 rpm. Most of the region of the corrosion film formed at 0 rpm was intact. However, the corrosion film in some areas was peeled because of the high rotation rate. The EDS results revealed that O and Cr contents increased and that the Fe content decreased compared with that formed under a static condition. It seems that the increasing rotation rate accelerated the enrichment of $Cr(OH)_3$ in the corrosion film. Moreover, the high rotation rate could cause mechanical damage to the corrosion film. However, the EDS results (Fig. 10f) indicated that the area where corrosion film was peeled was still covered with a Cr-rich corrosion film. Therefore, R_{pore} and R_p measured at 1000 rpm increased slowly; however, they were still higher than that measured at 0 rpm (Fig. 4).

Fig. 10c reveals the appearance of a grinding crack in the steel surface under 2000 rpm. However, the steel surface was still covered by a corrosion film with a typical cracked line. The EDS result indicates that the Fe content increased and the O and Cr contents decreased compared to that at low rotation rates. However, the corrosion film was still enriched in $Cr(OH)_3$. The main reason for this irregularity may be that the corrosion film was too thin; thus, X-rays penetrated the corrosion film and detected the signal from the matrix.

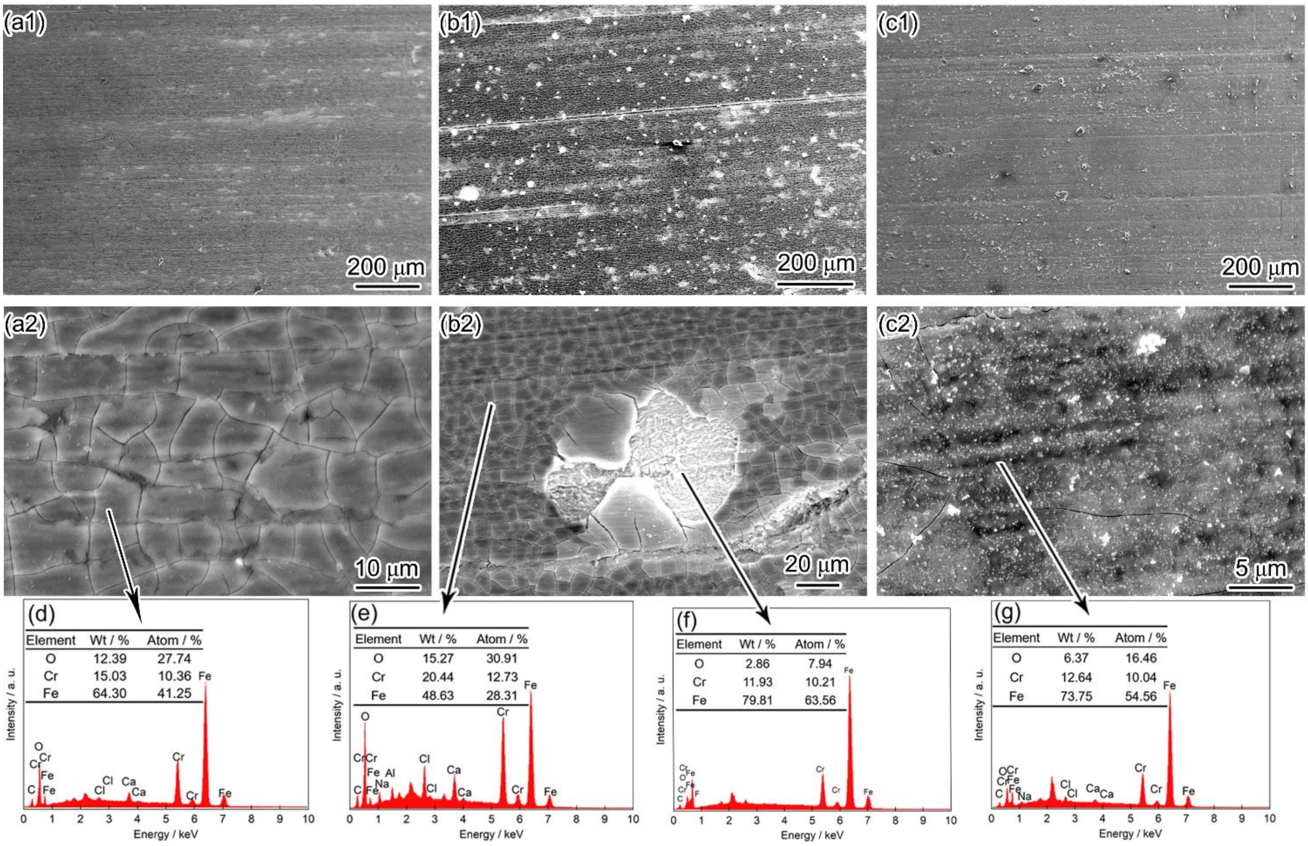

(d)

Element	Wt / %	Atom / %
O	12.39	27.74
Cr	15.03	10.36
Fe	64.30	41.25

(e)

Element	Wt / %	Atom / %
O	15.27	30.91
Cr	20.44	12.73
Fe	48.63	28.31

(f)

Element	Wt / %	Atom / %
O	2.86	7.94
Cr	11.93	10.21
Fe	79.81	63.56

(g)

Element	Wt / %	Atom / %
O	6.37	16.46
Cr	12.64	10.04
Fe	73.75	54.56

Figure 10. SEM and EDS analysis of corrosion film of 6.5Cr steel after immersion for 24 h under different rotation rates （a）（d）0 rpm;（b）（e）（f）1000 rpm;（c）（g）2000 rpm

3.5. Mechanism analysis

Because the corrosion rate decreased with the increasing rotation rate (Fig. 6), the sequence of the total Fe^{2+} content was as follows: $C(Fe^{2+})_{\text{total, 0 rpm}} > C(Fe^{2+})_{\text{total, 1000 rpm}} > C(Fe^{2+})_{\text{total, 2000 rpm}}$. The ICP test was performed to measure the Fe^{2+} content in the solution after 24 h immersion. Fig. 11 indicates that the sequence of the Fe^{2+} content in the solution was as follows: $C(Fe^{2+})_{sol,\ 1000\ rpm} > C(Fe^{2+})_{sol,\ 0\ rpm} > C(Fe^{2+})_{sol,\ 2000\ rpm}$. Furthermore, EDS results revealed that the Cr/Fe ratio of the corrosion product generated at 1000 rpm was higher than 0 rpm. When the rotation rate increased from 0 rpm to 1000 rpm, the Fe^{2+} tend to dissolve into the solution and was less deposited in the corrosion film, which leads to the enrichment of $Cr(OH)_3$ in the corrosion film. It is generally considered that the Cr/Fe ratio and the enrichment of $Cr(OH)_3$ in corrosion film is closely related to the corrosion resistance of low-Cr alloy steel [14,28,31-33].

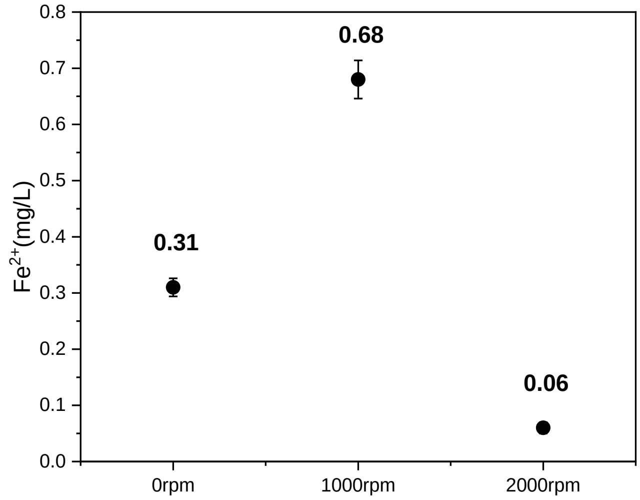

Figure 11. The Fe^{2+} content in the solution under different rotation rates.

From the results of 0 rpm and 1000 rpm, it can be inferred that the deposition of $FeCO_3$ was more difficult after the rotation rate was increased, and the influence of rotation rate on the generation of $Cr(OH)_3$ was less substantial than that of $FeCO_3$, thus leading to an increase in the enrichment of $Cr(OH)_3$ in the corrosion film.

However, the lowest Fe^{2+} concentration was observed at 2000 rpm due to the low corrosion rate. And the corrosion film was extremely thin; thus, the EDS results could not verify the accuracy of the aforementioned speculation at 2000 rpm. The results are not consistent with the aforementioned assumption. To validate the aforementioned assumption, the following experiments were conducted. The 6.5Cr steel was immersed at 0 rpm for 1 h, at 1000 rpm for 1 h, and at 2000 rpm for 24 h. The OCP and EIS were monitored during the immersion test.

The shape of OCP curve(Fig. 12a) was similar to that at 1000 rpm. However, the OCP was more positive than that at 1000 rpm and more negative than that at 2000 rpm. The changes in EIS results (Fig. 12b) were also similar to those at 1000 rpm, showing a trend of transition from a double capacitive reactance arc to a high-frequency capacitive reactance arc, medium-frequency inductive reactance arc, and low-frequency capacitive reactance arc, which differed considerably from that at 2000 rpm. Fig. 12c reveals that the morphology of the corrosion film was similar to that of 1000 rpm. The EDS result (Fig. 12d) indicated that the Cr/Fe ratio increased compared with that of 1000 rpm, which validated the accuracy of the aforementioned assumption that the increasing of flow rate can promote the enrichemnt of $Cr(OH)_3$.

In addition, the results also suggested that a corrosion film generated at the initial stage considerably affected the property of the subsequent film under the conditions with a high rotation rate. Therefore, although the protective performance of the corrosion film deposited on the surface was improved, the film could not be converted into the passivation film under a high rotation rate due to the generation of corrosion film with a low percentage of $Cr(OH)_3$ at the initial stage. The protective performance of this corrosion film was still considerably worse than that formed at a high rotation rate from the beginning.

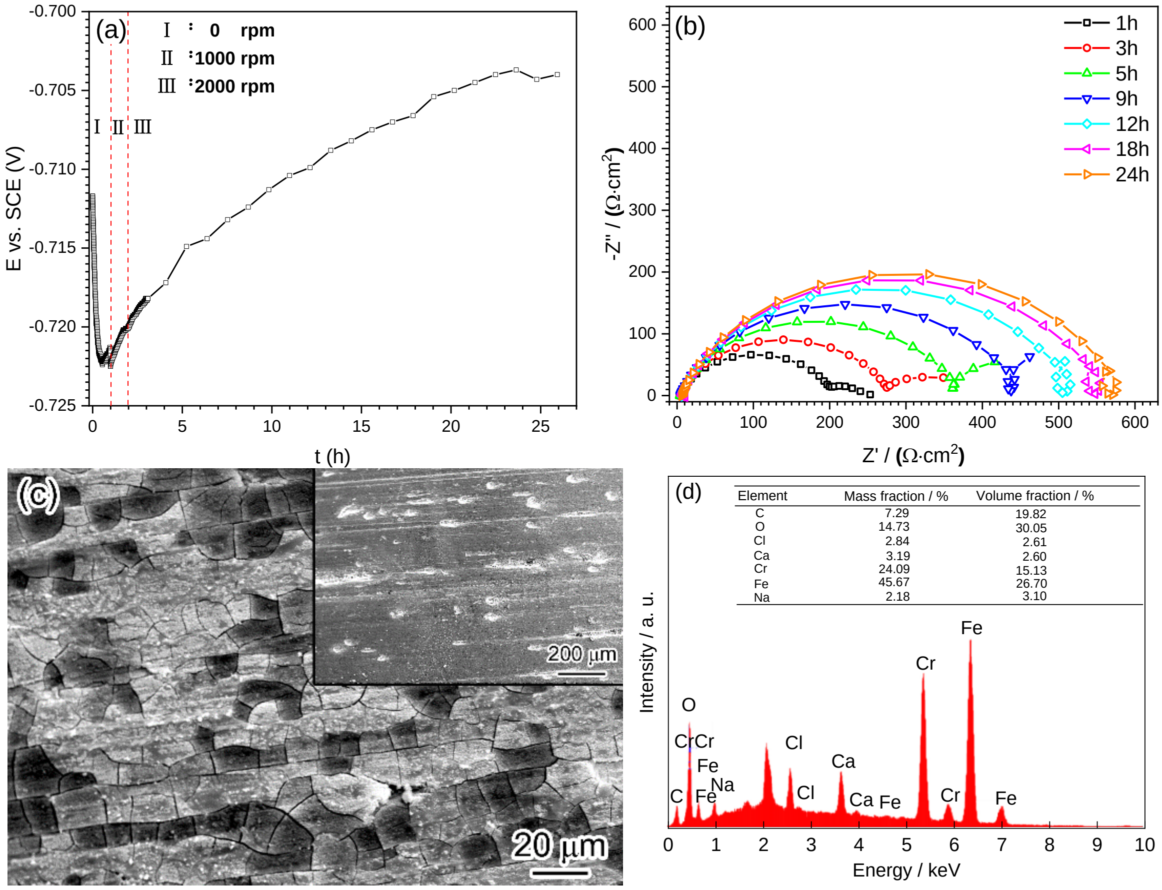

Element	Mass fraction / %	Volume fraction / %
C	7.29	19.82
O	14.73	30.05
Cl	2.84	2.61
Ca	3.19	2.60
Cr	24.09	15.13
Fe	45.67	26.70
Na	2.18	3.10

Figure 12. The results of 6.5Cr steel immersed at 0 rpm for 1 h, at 1000 rpm for 1 h, and at 2000 rpm for 24 h. (a) OCP; (b) EIS; (c) SEM; (d) EDS

In conclusion, the corrosion mechanism of 6.5Cr steel under the high rotation rate is as follows: The anodic reaction of 6.5Cr in the CO_2-saturation solution primarily included the dissolution of Fe and Cr through multiple steps [Eqs. (2–7)][38,39]:

$$Fe+H_2O \rightarrow FeOH_{ad}+H^{+}+e^{-} \quad (2)$$

$$FeOH_{ad} \rightarrow FeOH^{+}+e^{-} \quad (3)$$

$$FeOH^{+}+H^{+}\rightarrow Fe^{2+}+H_2O \qquad (4)$$

$$Cr+H_2O\rightarrow CrOH_{ad}+H^{+}+e^{-} \qquad (5)$$

$$CrOH_{ad}\rightarrow CrOH^{+}+e^{-} \qquad (6)$$

$$CrOH^{+}+H^{+}\rightarrow Cr^{3+}+H_2O+e^{-} \qquad (7)$$

Fig. 13a shows that intermediate products FeOH and CrOH were formed and adsorbed on the steel surface, and an abundance of Fe^{2+} and Cr^{3+} ions were observed in the near surface of 6.5Cr steel at the initial stage. Then, Fe^{2+} was precipitated as $FeCO_3$ [Eqs. (8)][40]. The Cr^{3+} ions were hydrolysed into $Cr(OH)_3$ [Eqs. (10)] [37,41].

$$Fe^{2+}+CO_3^{2-}\rightarrow FeCO_3\downarrow \qquad (8)$$

$$Cr^{3+}+3H_2O\rightarrow Cr(OH)_3\downarrow + 3H^{+} \qquad (9)$$

Because of the hydrolyzation of Cr^{3+} ions, the near-surface solution was acidified, and the anodic reaction was accelerated [25,28]. Therefore, the OCPs of the samples at 0 and 1000 rpm decreased at the initial stage (Fig. 1).

Fig. 13b shows that for 0 rpm, Fe^{2+} ions near the surface can only be diffused in the solution in accordance with the concentration gradient, and the diffusion velocity was considerably lower than that of convection-diffusion. Therefore, the Fe^{2+} ions near the surface had a higher concentration [25,28], and the $FeCO_3$ in the corrosion film had the highest proportion and lowest level of protection. Fig. 14 reveals that for 0 rpm, the cathode polarization curve intersected with the anode polarization curve in the activation region; thus, the apparent polarization curve presented pseudopassivation characteristics without a stable passivation region.

Fig. 13c shows that because of strong convective diffusion, Fe^{2+} ions migrated to the solution, and the concentration of Fe^{2+} ions near the surface sharply decreased when the rotation rate increased to 1000 rpm. Because of the lower Ksp value of $Cr(OH)_3$, Cr^{3+} ions could be easily hydrolyzed into $Cr(OH)_3$ and deposited on the steel surface [42]. Therefore, fewer Cr^{3+} ions than Fe^{2+} ions migrated to the solution from the near-surface, which resulted in the enrichment of $Cr(OH)_3$ in the corrosion film. Besides, some studies indicated that $Cr(OH)_3$ is likely to grow in situ rather than dissolve first and then deposit on the steel surface [43]. Similar results have been reported in the literature. Motta [22] found that the precipitation rate of $FeCO_3$ reduces for a higher velocity, and a high flow rate can promote the redissolution of the deposited $FeCO_3$. The corrosion resistance of the $Cr(OH)_3$ was considerably superior to that of $FeCO_3$ at flowing conditions, and it provided suitable protection for the matrix and reduced the corrosion rate. Fig. 14 showed that compared with 0 rpm, because of the deposition of this corrosion film with a high Cr content, the anodic polarization curve shifted to the left and intersected with the cathodic polarization curve in the activation region. Therefore, the corrosion current density decreased, and the corrosion potential increased; however, the apparent polarization curve still exhibited a pseudopassivation characteristic without a stable passivation region.

Fig. 13d shows that when the rotation rate was increased to 2000 rpm, the convective diffusion was considerably stronger, causing the majority of Fe^{2+} to dissolove into the solution. The formation of this corrosion film was rapid, and its thickness was low; however, the percentage of $Cr(OH)_3$ in the generated corrosion film was considerably increased. Studies have shown that for low-Cr alloy steel when the corrosion film is highly enriched in $Cr(OH)_3$, the film is similar to the passivation film of stainless steel [32]. Because of the formation of this film, the anode polarization curve shifted to left and intersected with the cathode polarization curve in the passivation zone [31]. Therefore, the OCP at the initial stage of corrosion rapidly increased, and the apparent polarization curve exhibited passivation characteristics, thus significantly decreasing the corrosion rate under this condition.

In conclusion, for 6.5Cr steel, high flow rate can reduce the Fe^{2+} concentration in the solution near the steel surface, thus inhibiting the deposition of $FeCO_3$, enriching $Cr(OH)_3$ in the corrosion film, promoting the passivation of the steel, and increasing the protection property of the corrosion film.

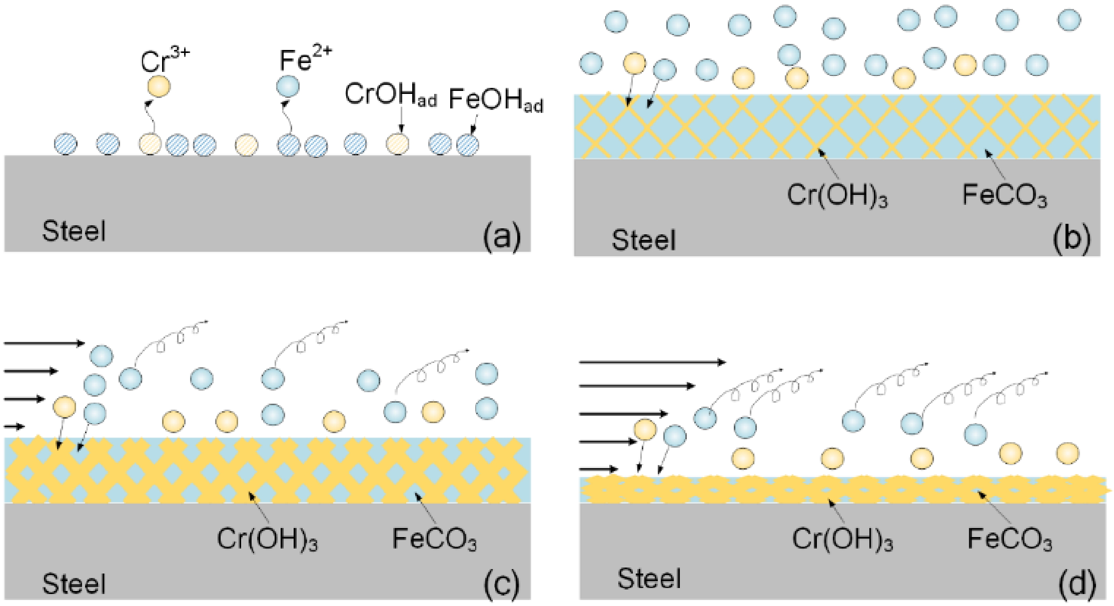

Figure 13. Schematic of the corrosion film formation of 6.5Cr steel in a CO_2-containing environment with different rotation rates. (a) Initial stage, (b) 0 rpm, (c) 1000 rpm, (d) 2000 rpm

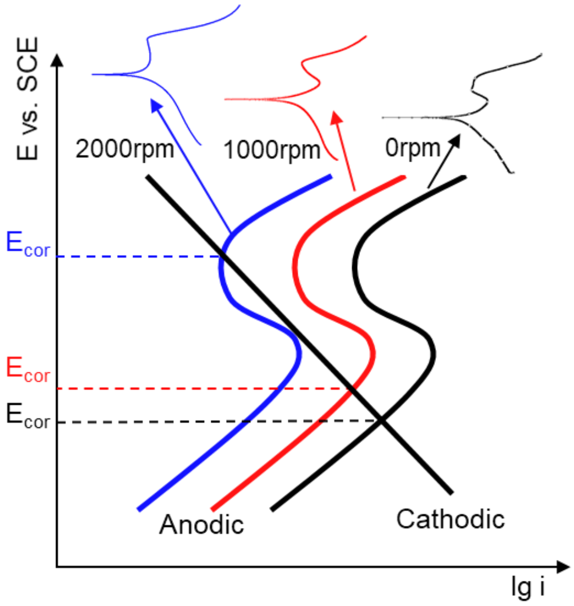

Figure 14. Evans diagram for 6.5Cr steel at different rotation rates

5. CONCLUSIONS

The effect of turbulent flow on the corrosion behavior of 6.5Cr steel was studied using the RCE. The principal conclusions are as follows:

(1)An increase in the flow rate (0–2000 rpm) could enhance the corrosion resistance of 6.5Cr steel in a CO_2-containing environment.

(2)When the rotation rate of the RCE was 2000 rpm, 6.5Cr steel was passivated, and its corrosion rate sharply decreased.

(3)For 6.5Cr steel, an increase in the flow rate could reduce the Fe^{2+} concentration in the solution near the steel surface, thus inhibiting the deposition of $FeCO_3$, enriching $Cr(OH)_3$ in the corrosion film, promoting the passivation of the steel, and increasing the protection perperty of the corrosion film.

(4)The corrosion film deposited at the initial stage had a strong influence on the deposition and properties of the subsequent scale under high rotation rates.

ACKNOWLEDGEMENT
The project is supported by China Postdoctoral Science Foundation (Grant No. 2019M660454).

References

1. F. Farelas, M. Galicia, B. Brown, S. Nesic, and H. Castaneda, *Corros. Sci.*, 52 (2010) 509-517.
2. E.T. Heakal, and A.E. Elkholy, *J. Mol. Liq.*, 230 (2017) 395-407.
3. M.A. Hegazy, A.Y. El-Etre, M. El-Shafaie, and K.M. Berry, *J. Mol. Liq*, 214 (2016) 347-356.
4. S. Mokhatab, W.A. Poe, and J.Y. Mak, Elsevier, (2015) Amsterdam, NL.
5. P. Kannan, T.S. Rao, and N. Rajendran, *J. Colloid. Interf. Sci.*, 512 (2017) 618.
6. K.M. Usher, A.H. Kaksonen, I. Cole, and D. Marney, *Int. Biodeter. Biodegr.*, 93 (2014) 84-106.
7. G.A. Zhang, and Y.F. Cheng, *Corros. Sci.,* 52 (2010) 2716-2724.
8. G.A. Zhang, L. Zeng, H.L. Huang, and X.P. Guo., *Corros. Sci.*, 77 (2013) 334-341.
9. X. Jiang, Y.G. Zheng, and W. Ke, *Corros. Sci.*, 47 (2005) 2636-2658.
10. A. Prethaler, G. Mori, and E. Rosenberg, *BHM Berg- Huttenmann. Monatsh*, 160 (2015) 346-351.
11. Q. Wu, Z. Zhang, X. Dong, and J. Yang, *Corros. Sci.*, 75 (2013) 400–408.
12. M.N. Zafar, R. Rihan, and L. Al-Hadhrami, *Corros. Sci.*, 94 (2015) 275–287.
13. S. Hassani, T.N. Vu, N.R. Rosli, S.N. Esmaeely, Y.S. Choi, D. Young, and S. Nesic, *Int. J. Greenh. Gas Con.*, 23 (2014) 30–43.
14. L.N. Xu, B. Wang, J.Y. Zhu, W. Li, and Z.Y. Zhen, *Appl. Surf. Sci.*, 379 (2016) 39-46.
15. L.N. Xu, J.Y. Zhu, and B. Wang, *Acta. Metall. Sin.*, 53 (2017) 677-683.
16. S.Q Guo, L.N. Xu, L. Zhang, W. Chang, and M.X. Lu, *Corros. Sci.*, 110 (2016) 123-133.
17. Y. Xie, L.N. Xu, C. Gao, W. Chang, and M.X. Lu, *Mater. Des.*, 36 (2016) 54–57.
18. C.F. Chen, M.X. Lu, D. Sun, Z. Zhang, and W. Chang, *Corros.,* 61 (2005) 594–601.
19. Z.Q. Bai, C.F. Chen, M.X. Lu, and J.B. Li, *Appl. Surf. Sci.*, 252 (2006) 7578–7584.
20. L.H. Hu, L. Zhang, W. Chang, and M.X. Lu, *J. Univ. Sci. Technol. B.*, 32 (2010) 345–350.
21. K. Nose, J.W. Martin, H. Asahi, and P.I. Nice, presented at NACE Internatioal-Corrosion Conference and Expo, Houston, USA, 2001, paper no. *82*.
22. R.A. De Motta, University of Leeds, (2016) Leeds, UK.
23. S. Nešić, *Corros. Sci.*, 49 (2009) 4308-4338.
24. Y. Yang, B. Brown, S. Nešić, M.E. Gennaro, and B. Molinas, presented at NACE Internatioal-

Corrosion Conference and Expo, Houston, USA, 2010, paper no. 10383.
25. L.N. Xu , S.Q. Guo, W. Chang, T.H. Chen, L.H. Hu, and M.X. Lu, *Appl. Surf. Sci*., 270 (2013) 395-404.
26. S. Jiang, F. Chai, H. Su, and C.F. Yang, *Corros. Sci*., 123 (2017) 217-227.
27. F. Chai, S. Jiang, and C. Yang, *J. Iron. Steel. Res. Int*., 23 (2016) 602-607.
28. J. Y. Zhu, L.N. Xu, M.X. Lu, L. Zhang, W. Chang, and L.H. Hu, *Corros. Sci*., 93 (2015) 336-340.
29. H.Z. Hong, L.J. Wang, J.K. Sun, W.J. Liiu, and Z.W. Wang, Int. *J. Electrochem. Sci.*, 15 (2015) 6596-6604.
30. I.Z. Machael, S.R. Allahkaram, and H.A. Ramezani-Varzaneh, *Corros. Sci*., 157 (2019) 472-480.
31. B. Wang, L.N. Xu, J. Y. Zhu, H. Xiao, and M.X. Lu, *Corros. Sci*., 111 (2016) 711-719.

32. L. Wei, University of Science and Technology Beijing, (2016) Beijing, CHN.
33. L. Wei, K. Gao, *J. Alloys Compd.*, 792 (2019) 328-340.
34. G.S. Vasyliev, *Corros. Sci*., 98 (2015) 33-39.
35. K. Denpo, and H. Ogawa, *Corros.*, 49 (1993) 442-449.
36. B. Wang, L.N. Xu, G. Z. Liu, and M.X. Lu, *Corros. Sci*., 136 (2018) 210-220.
37. T.H. Chen, L.N. Xu, M.X. Lu, W. Chang, and L. Zhang, presented at NACE Internatioal-Corrosion Conference and Expo, Houston, USA, 2011, paper no. 11074.
38. J.O. Bockris, D. Drazic, and A.R. Despic, *Electrochim. Acta,* 4 (1961) 325-361.
39. J. Y. Zhu, L.N. Xu, and M.X. Lu, , *Corrosion*, 71 (2015) 854-864.
40. T. Muraki, K. Nose, and H. Asahi, presented at NACE Internatioal-Corrosion Conference and Expo, Houston, USA, 2003, paper no. 117.
41. J.B. Sun, W. Liu, W. Chang, Z. Zhang, Z. Li, T. Yu, and M.X. Lu, *Acta Metall. Sin.*, 45 (2009) 84-90.
42. Y. Zhao, X. Li, C. Zhang, T. Zhang, J. Xie, G. Zeng, D. Xu, and F. Wang, *Corros. Sci*., 145 (2018) 307-319.
43. L.N. Xu, B. Wang, and M.X. Lu, *Acta Metall. Sinica*, 52 (2016) 672-678.